Hard sphere fluids in random fiber networks

Matthias Schmidt[a)]
Soft Condensed Matter, Debye Institute, Utrecht University, Princetonpln 5, 3584 CC Utrecht,
The Netherlands

Joseph M. Brader
Institute of Physiology, University of Bern, Buehlplatz 5, 3012 Bern, Switzerland

We investigate an annealed hard sphere fluid in contact with a rigid, random fiber network modeled by quenched, vanishingly thin hard needles. For this model a quenched-annealed density functional theory is presented that treats arbitrary spatially inhomogeneous situations, in particular anisotropic and spatially varying needle distributions. As a test case we consider the structure of the hard sphere fluid at the surface of an isotropic fiber network and find good agreement of the theoretical density profiles with our computer simulation results. For high needle densities the surface acts like a rough impenetrable wall. In the limit of infinite needle density the behavior near a smooth hard wall is recovered. Results for the partition coefficient agree well with existing data. © *2003 American Institute of Physics.* [DOI: 10.1063/1.1588993]

I. INTRODUCTION

The properties of fluids adsorbed in porous media can be drastically different from those of the same substance in bulk.[1] Among the wide range of disordered adsorbents one particular class are aggregates of mesoscopic fibers, such as those present in paper and in colloidal suspensions.[2,3] Due to their geometrical properties the solid volume fraction of fiber networks can be remarkably low. Experimentally, suspensions of rods can be prepared such that the particles are practically immobilized (e.g., by sedimentation or coagulation) producing a random network of fibers. The resulting gels or clusters of colloidal rods or fibers were found to exhibit both homogeneous and heterogeneous (i.e., fractal) structures.[4] One prominent material where the structure of the rod gel has been investigated is aqueous dispersions of colloidal boehmite.[5] Other examples of gels of fairly well-defined colloidal rods are iron hydroxide rods, clay particles, and imogolite rods (see Ref. 4). Further very promising particles are etched silicon rods.[6]

Fiber networks provide genuine model porous media that can be used to address various relevant physical questions like the self-diffusion and sedimentation of (tracer) spheres.[7] Particularly striking is the efficiency of randomly distributed thin rods to cage a test sphere.[8] Sphere caging is relevant for the random dense sphere packing.[9] Dense rod packing has been investigated and a random contact equation was found to be relevant,[10] and packings of spherocylinders were simulated recently by mechanical contraction.[11] Furthermore, the spatial statistics of pore sizes in stochastic fiber networks was investigated.[12,13]

Experimental rod aspect ratios (of length-to-thickness) can be as high as 25 for silica coated boehmite rods, and the rod densities are typically well below the Onsager nematic–isotropic transition.[3] Under equilibrium conditions (i.e., such that rods are mobile) also mixtures have been considered, e.g., silica spheres[3] were added and also immersed in suspensions of rod-like fd bacteriophage viruses.[14] For a simple theoretical model of hard spheres and vanishingly thin needles the phase behavior was obtained with computer simulations and perturbation theory.[15] Fluids in contact with a single[16,17] and several strictly aligned[18] rod-like obstacles were treated theoretically finding intriguing adsorption behavior.[18] A molecular model of adsorption in a semiflexible porous network was simulated[19] taking into account structural response of the adsorbent.

The pore size distribution in a random fiber network was derived by Ogston in his classical work[20] (see Ref. 21 for brief personal recollections). This solution rules the adsorption probability of an infinitely diluted hard sphere fluid in a bulk fiber network. In the present work we are interested in the adsorption of a dense fluid in a random network of rods. We treat an annealed hard sphere fluid immersed in a quenched network of vanishingly thin hard needles. This model can be viewed as the quenched-annealed (QA) analog of the above equilibrium sphere-needle mixture.[15] In particular we address the question how the geometry of the quenched particles affects the properties of such a network to act as an adsorbent.

We use density-functional theory (DFT),[22,23] which is a powerful tool to study inhomogeneous fluids. In particular, Rosenfeld's fundamental measure theory (FMT) for hard sphere mixtures[24] is known for its high accuracy (for very recent work see, e.g., Refs. 25 and 26). Rosenfeld generalized his approach to nonspherical particles,[27,28] albeit without incorporating the exact low-density (second virial) limit. Introducing angular convolutions into the theory enabled this exact limit to be recovered in binary mixtures of hard sphere and hard rods with either ideal (vanishing)[29] or residual excluded volume interactions (Onsager limit).[30] Using this

[a)]On leave from: Institut für Theoretische Physik II, Heinrich-Heine-Universität Düsseldorf, Universitätsstraße 1, D-40225 Düsseldorf, Germany; Electronic mail: mschmidt@thphy.uni-duesseldorf.de

3495

theory interesting orientational order at the free fluid–fluid interface between demixed phases was found,[30] and later supported by computer simulation results.[31]

To investigate the response of fluids to external confinement there are two main theoretical routes: First, one relies on idealized pore geometries, i.e., slit-like, cylindrical, or spherical pores with smooth walls.[32] The insights gained here are then related to the behavior in random media by identifying typical pore sizes that are characteristic of the amorphous void structure. An example of this strategy is Fanti and Glandt's investigation of the partitioning of spherical particles into fibrous matrices[16] where the problem of a single fiber is solved explicitly and then related to a network of fibers via a superposition approximation. The second approach is to model the porous medium by immobilized configurations of model fluids. Then an adsorbate component is equilibrated (i.e., annealed) in the presence of the model porous medium, that acts like an external potential on the adsorbate. One refers to such models as quenched-annealed (QA) mixtures. While the first approach can be viewed as a *raison-d'être* of DFT, the second route was primarily followed by use of integral equation theory and application of the replica trick, e.g., Dong *et al.* derived the inhomogeneous replica Ornstein–Zernike equations to treat problems like the adsorption near a plane boundary of a disordered matrix.[33]

For QA mixtures a DFT framework was proposed recently.[34] The benefit of this QA DFT is that the disorder is treated on the level of the one-body density distribution of the quenched species, rather than as a complicated external field (like, e.g., in Ref. 18). The one-body density has (in typical situations) a much simpler spatial dependence than the corresponding external potential that is exerted by the matrix particles on the adsorbate. As an illustration we remark that in a (bulk) matrix that is uniform on average over the disorder, the matrix one-body density is just a constant.

In this work we propose a QA DFT for the mixture of annealed spheres and quenched needles and test it against our computer simulation results. As a generic inhomogeneous situation we consider the surface of an isotropic needle network. We bring a dense hard sphere fluid in contact with this surface and investigate the structure that is built up as a response to the quenched needles. Comparing theoretical and simulated results we find that the plateau values away from the matrix surface deviate somewhat, but the detailed oscillatory structure at the interface is captured very well by the DFT. For high needle densities the network becomes practically impenetrable for the spheres, and the surface acts as a rough wall. Within the QA DFT the surface roughness is treated very easily, in particular it is not necessary to treat the lateral structure of the surface explicitly. Hence the computational effort is similar to that for treating a smooth wall. We find that the surface roughness decreases with increasing needle density and effectively a hard smooth wall is obtained in the limit of infinite needle density. Furthermore we check that our results for the partition coefficient compare reasonably to previous Monte Carlo results.[17]

The remainder of the paper is organized as follows: In Sec. II we define the model of hard spheres in a random fiber network more explicitly. Section III is devoted to an outline
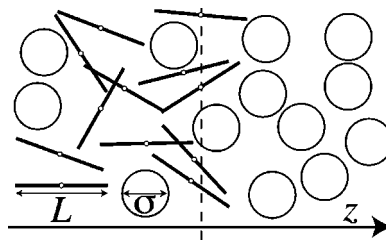
FIG. 1. Model of an adsorbate fluid of hard spheres with diameter σ in a porous matrix of quenched, vanishingly thin hard needles of length L. The needle orientations are assumed to be isotropically distributed and their midpoints to be confined to the halfspace $z < 0$. This generates a semi-infinite porous matrix with surface perpendicular to the z axis and located at $z = 0$; the model considered is three-dimensional.

of the density functional theory. Section IV gives details of the computer simulations. Results are presented in Sec. V and we conclude in Sec. VI.

II. THE MODEL

We consider annealed hard spheres (species S) of diameter σ immersed in a quenched matrix of vanishingly thin needles (species N) of length L. The model is characterized by the (three) pair interactions V_{ij} between species $i,j = S,N$. Due to their vanishing thickness (and hence vanishing pair excluded volume) the needles behave as if being ideal, hence interactions between needles vanish for all separation distances and orientations, $V_{NN} = 0$. The interaction between spheres is $V_{SS}(r) = \infty$ if the separation r between sphere centers is less than σ, and zero otherwise. The pair interaction between a sphere and a needle is $V_{SN} = \infty$, if both overlap, and zero otherwise.

As thermodynamic variables we use the sphere packing fraction $\eta = \pi \sigma^3 \rho_S / 6$, and a dimensionless needle density $\rho_N \sigma^3$, where $\rho_i, i = S,N$ is the number density of species i. The size ratio L/σ is a further (geometric) control parameter. In general the one-body density distributions will be inhomogeneous. In the case of spheres, dependence is on space point $\mathbf{r}$, hence $\rho_S(\mathbf{r})$. For needles the dependence is also on orientation $\mathbf{\Omega}$ (a unit vector), hence $\rho(\mathbf{r},\mathbf{\Omega})$.

As a generic inhomogeneity we will consider the surface of a needle matrix modeled as a step-function density distribution,

$$\rho_N(\mathbf{r},\mathbf{\Omega}) = \rho_N^{\text{in}} \Theta(-z), \tag{1}$$

where z is the spatial coordinate perpendicular to the matrix surface, ρ_N^{in} is the needle density "inside" the matrix, and we consider the (simplest) case where the needles are isotropically distributed. See Fig. 1 for an illustration of the situation.

III. DENSITY FUNCTIONAL THEORY

We seek a theory to determine the adsorbate (sphere) density distribution $\rho_S(\mathbf{r})$ (as well as associated thermodynamic quantities and correlation functions) for given one-body density distribution of needles, $\rho_N(\mathbf{r},\mathbf{\Omega})$. As the needles are treated as being ideal, $\rho_N(\mathbf{r},\mathbf{\Omega})$ can be trivially obtained from a corresponding external potential acting on

needles (before quenching). Within a DFT framework and following Ref. 34 we write the grand potential of the present QA mixture as

$$\Omega[\rho_S;\rho_N]=k_BT\int d\mathbf{r}\rho_S(\mathbf{r})[\ln(\rho_S(\mathbf{r})\Lambda_S^3)-1]$$

$$+F_{\mathrm{exc}}[\rho_S(\mathbf{r});\rho_N(\mathbf{r},\mathbf{\Omega})]$$

$$+\int d\mathbf{r}\,\rho_S(\mathbf{r})[V_S^{\mathrm{ext}}(\mathbf{r})-\mu_S], \qquad (2)$$

where k_B is the Boltzmann constant, T is absolute temperature, Λ_S is the thermal wavelength, μ_S is the chemical potential of spheres, and $V_S^{\mathrm{ext}}(\mathbf{r})$ is a deterministic (nonrandom) external potential acting on the spheres. The first term on the right-hand side of Eq. (2) is the ideal gas free energy functional for spheres; the second term, F_{exc}, is the excess free energy describing the contributions from interparticle interactions. In the present QA case it contains the interactions between adsorbate particles (spheres and spheres), as well as contributions from interactions between adsorbate and matrix particles (spheres and needles).

To obtain the adsorbate density distribution, $\rho_S(\mathbf{r})$, in a given needle matrix, $\rho_N(\mathbf{r}',\mathbf{\Omega})$, the minimization condition is

$$\left.\frac{\delta\Omega}{\delta\rho_S(\mathbf{r})}\right|_{\rho_N(\mathbf{r}',\mathbf{\Omega})}=0, \qquad (3)$$

where $\rho_N(\mathbf{r}',\mathbf{\Omega})$ is treated as a fixed input quantity. Note that, in contrast to the case of an equilibrium (fully annealed) binary mixture, the minimization is to be performed only with respect to the annealed component.

In order to obtain a working theory an approximation for the unknown quantity in Eq. (2), the Helmholtz excess free energy functional F_{exc}, is required. Recently, this was accomplished for spherical particles in a geometrical framework. This provides a means to generate a three-dimensional excess free energy functional from an idealized strongly confined situation, the zero-dimensional (0D) limit. The 0D limit can be envisaged as a cavity situation that leads to strongly localized particle positions. The simplification that is due to the localization enables one to solve the many-body problem exactly and to obtain the corresponding 0D free energy. For the present case, it was shown that for a binary system of hard spheres (one annealed and one quenched species), F_{exc} is (practically) equal to the fully equilibrated case with only annealed species. The only difference is a shift by a trivial constant, $F_{\mathrm{exc}}^{\mathrm{QA}}[\rho_0,\rho_1]=F_{\mathrm{exc}}^{\mathrm{EQ}}[\rho_0,\rho_1]-F_{\mathrm{exc}}^{\mathrm{EQ}}[\rho_0]$, where the subscript 0 (1) refers to the quenched (annealed) component. Note that the presence of $-F_{\mathrm{exc}}^{\mathrm{EQ}}[\rho_0]$ on the right-hand side is necessary to fulfill $F_{\mathrm{exc}}^{\mathrm{QA}}[\rho_0,\rho_1\rightarrow0]=0$, i.e., the (over disorder averaged) free energy vanishes in the absence of adsorbate particles. However, this does not change the minimization condition, as the functional derivative is only performed with respect to the *annealed* component, cf. Eq. (3).

For the present case of quenched needles and annealed spheres an additional simplification arises, because the needles behave as ideal particles due to their geometry. The excess free energy of an ideal gas of rotators vanishes, hence
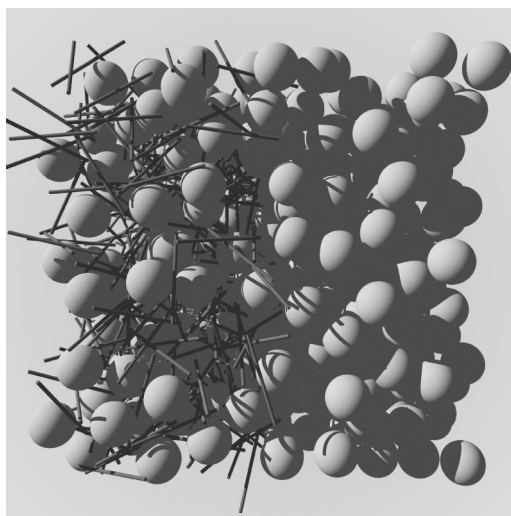
FIG. 2. Snapshot from computer simulation of the adsorbate hard sphere fluid in contact with a random fiber network. The fiber network is modeled as randomly and isotropically distributed vanishingly thin hard needles. Only the left part of the (periodic) simulation box is filled with needles; this acts as a model for the surface of a porous medium. The size ratio of needle length L and sphere diameter σ is $L/\sigma=2$; particle numbers are $M_S=M_N=512$.

we find that the FMT approximation for F_{exc} is *equal* to the excess free energy of the fully annealed sphere-needle mixture given in Ref. 29. The main features of this theory are density-independent, geometrically motivated weight functions that are used to build weighted densities by convolutions with the bare one-body densities. The excess free energy is then obtained as an integral that runs over space and orientation, the integrand being an excess free energy density that is a function of the weighted densities. For explicit expressions we refer the reader directly to the (compact) presentation in Ref. 29; many more technical details and explicit calculations in simple geometries can be found in Ref. 30.

IV. COMPUTER SIMULATIONS

In order to assess the quality of the DFT results we have carried out canonical Monte Carlo (MC) simulations. We used particle numbers $M_S=M_N=128$, 512, and a cubic simulation box with length L and periodic boundary conditions. The size ratio was fixed to $L/\sigma=2$. Needle configurations were generated by randomly and isotropically placing needles in the left ($-L/2<z<0$) half of the simulation box. Due to the periodic boundary conditions *two* matrix surfaces are generated. As an illustration we display in Fig. 2 a ray-traced snapshot from the simulation. For the state points considered the two surfaces are not completely decoupled, hence we merely deal with a periodic succession of slabs filled with needles and slabs free of needles. Hence the "free slab" has thickness $L/2$ and the "matrix slab" has also thickness $L/2$. For $M_S=128$ and $\eta=0.15$, 0.3, the box lengths are $L/\sigma=7.64491$, 6.06777, respectively. For $M_S=512$, and $\eta=0.15$, 0.3 the box lengths are $L/\sigma=12.1355$, 9.63198, respectively. As we consider equal numbers of particles, $M_S=M_N$, the relation between densities is ρ_N^{in}
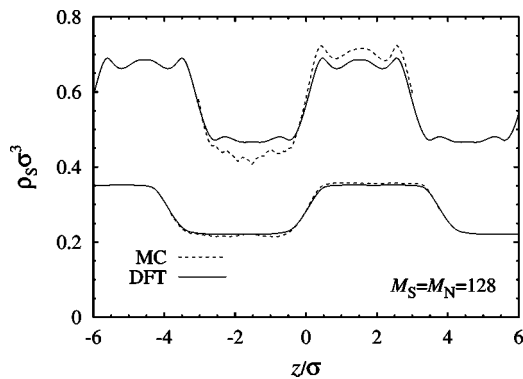
FIG. 3. One-body density distribution of spheres, $\rho_S(z)\sigma^3$, as a function of the (scaled) distance from the matrix surface, z/σ. Results from DFT (solid lines) and MC simulations (dashed lines) are shown for $\eta=0.15$, 0.3 (from bottom to top). The particle numbers in the simulated system are $M_S=M_N=128$.

FIG. 4. Same as Fig. 3, but for larger systems with $M_S=M_N=512$ particles.

$=2\eta_S/(\sigma^3\pi/6)$, where the factor 2 comes from the fact that only one half of the box is occupied by needles; hence $\rho_N\sigma^3=0.572\,958$, and $\rho_N\sigma^3=1.145\,92$.

In the starting configuration all spheres are placed in the half-space $z>0$, then half of the total number of particle moves are discarded for equilibration and subsequently data are collected for the sphere density profile. Typical run lengths are 10^6 MC moves per particle and averages over the disorder are taken by using about 100 matrix realizations. In the case of $\eta=0.3$, $M_S=128$ we performed 10^7 MC moves for 100 independent needle configurations totaling in 10^9 MC moves per particle.

V. RESULTS

To obtain the same situation as in the simulation we imposed the same periodicity L on the DFT profiles. The sphere packing fraction was matched to that in the simulation by adjusting the sphere chemical potential, μ_S in Eq. (2), such that the integrated sphere density corresponds to the simulated packing fraction, i.e., $\eta=(\pi\sigma^3/6)L^{-1}\int_{-L/2}^{L/2}dz\,\rho_S(z)$, where $\eta=0.15,0.3$.

In Fig. 3 we show results for the smaller system with $M_S=M_N=128$ particles. For $\eta=0.15$ there occurs a smooth crossover from the plateau value inside $(z<0)$ to the plateau value outside $(z>0)$ the matrix. There is almost perfect agreement between the simulated and the theoretical density profiles. For $\eta=0.3$ there occur oscillations both outside and also inside the matrix, albeit smaller in amplitude inside. The wavelength of oscillations is of the order of σ, hence caused by sphere packing effects. The shape of the theoretical results outside is very similar to the simulation result, however, it is shifted toward lower density. The opposite behavior is found inside the matrix, where the theoretical profile lies above the simulation result. Part of this may be due to still insufficient equilibration in the simulations, despite the considerably large number of MC moves performed.

In Fig. 4 we show results at the same state points, but for a larger system with $M_S=M_N=512$ particles. For $\eta=0.15$ again the agreement between simulation and theory is very good. For $\eta=0.3$ there is an increased number of layers
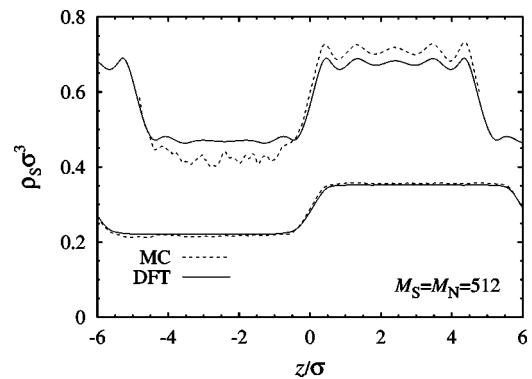
outside. The theory predicts weak oscillations inside the matrix, those cannot be identified from the simulation profiles—the statistical uncertainties being too large.

Having gained confidence in the theory, we consider a single surface of the fiber network, hence consider the case where the needles are distributed homogeneously and isotropically in the halfspace $z<0$. We bring this surface into contact with a hard sphere fluid of bulk packing fraction $\eta=0.4$ at $z\rightarrow\infty$. The size ratio is, as before, fixed to $L/\sigma=2$. For needle density $\rho_N\sigma^3=10$ practically no spheres can enter inside the matrix, and $\rho_S(z<0)$ vanishes on the scale of the plot, Fig. 5. The behavior of $\rho_S(z)$ near the surface, $0<z<\sigma/2$, is reminiscent of that of the hard sphere fluid at a soft repulsive wall. For larger z typical oscillations that decay with z are observed. Those possess a small amplitude, given the relatively high sphere packing fraction. Increasing the needle density (results for $\rho_N\sigma^3=100$, 1000, 10000 are shown in Fig. 5) gradually shifts $\rho_S(z)$ to larger z and increases the amplitude of the oscillations. These effects can be attributed to the denser, more "hairy" needle structure at the surface. It is evident that in the limit $\rho_N\rightarrow\infty$ the situation of an effective hard wall is encountered. The position of this effective hard wall is such that $\rho_S(z)$ drops to zero at $z=(L+\sigma)/2$ (for the present size ratio $z=1.5\sigma$), which is the limiting distance where spheres touch needles (those with orientation strictly perpendicular to the surface).
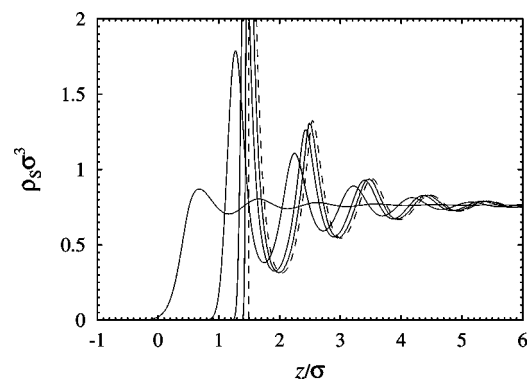
FIG. 5. Theoretical results for the density profiles $\rho_S\sigma^3$ as a function of z/σ from DFT for $\eta=0.4$, $L/\sigma=2$, and $\rho_N\sigma^3=10$, 100, 1000, 10 000 (from left to right). Also shown is the result at a hard smooth wall (dashed line).

We emphasize that the high needle densities considered here are somewhat artificial and only allowed by the present idealization of vanishing particle thickness. Networks of more realistic fibers with small, but *finite* thickness possess an upper bound in density for random isotropic packings.[10,11] This upper bound was estimated as $\rho_N L^2 D \pi/4 \approx 5.4$, where D is the rod thickness.[10] In experimental realizations aspect ratios are typically limited[11] to $L/D < 100$. If we assume this boundary (and $L/\sigma = 2$) then realistically (about) $\rho_N \sigma^3 < 100$. So the higher densities should be seen merely as an idealized crossover to the smooth hard wall behavior providing a convenient check for the theory.

We finish with a discussion of the adsorption of the hard sphere fluid deep inside the fiber network, i.e., away from the surface. The hard sphere fluid outside the matrix acts as a reservoir, and we denote its packing fraction by η^r. We seek to obtain the corresponding equilibrium sphere packing fraction η inside the matrix. Applying the DFT to constant density fields we find that the free energy per system volume is

$$\beta\Phi = \rho_S(\ln(\rho_S \Lambda_S^3) - 1) + \beta\Phi_{HS}(\eta)$$

$$+ \rho_N\left(-\ln(1-\eta) + \frac{3L\eta}{2\sigma(1-\eta)}\right), \quad (4)$$

where $\beta = 1/k_B T$, and Φ_{HS} is the excess free energy density in the Percus–Yevick compressibility (and scaled-particle theory) approximation, given by

$$\beta\Phi_{HS} = \frac{9\eta^2(2-\eta)}{\pi\sigma^3(1-\eta)^2} - \frac{6\eta}{\pi\sigma^3}\ln(1-\eta). \quad (5)$$

Then the sphere chemical potential is obtained by $\mu_S = \partial\Phi/\partial\rho_S$. Clearly, the situation is determined by chemical equilibrium of spheres outside and inside the matrix, hence we solve $\mu_S(\eta, \rho_N) = \mu_S(\eta^r, \rho_N = 0)$ for η once η^r and ρ_N are prescribed. This is an easy numerical task. Before presenting results for high packing fractions we investigate the behavior for $\eta \to 0$. It is straightforward to show that the leading order in this limit is $\beta\mu_S = \ln(\rho_S \Lambda_S^3) + \pi\rho_N \sigma^3(2 + 3L/\sigma)/12$. This is equivalent to Ogston's exact result,[20] i.e., the free volume fraction of a sphere in the needle matrix is obtained as the ratio of fugacities $\rho_S \Lambda_S^3/\exp(\beta\mu_S) = \exp(\rho_N \mathcal{E}_{SN})$, where $\mathcal{E}_{SN}$ is the pair-excluded volume between sphere and needle, given as $\mathcal{E}_{SN} = \pi\sigma^3/6 + \pi L\sigma^2/4$. (In Ref. 20 the derivative with respect to σ is given.) We next turn to the case of a dense adsorbate.

A common measure is the partition coefficient, that is defined as the ratio of adsorbed density and that in bulk, $K = \eta/\eta^r$. We first consider the case of infinitely long needles, $L/\sigma \to 0$, where benchmark results exist in the literature.[16,17] In Fig. 6 we plot K as a function of η^r for scaled needle densities $\rho_N L\sigma^2 = 0.1, 0.5, 1, 2, 3$. For all densities considered K is a monotonically increasing function of η^r, hence the partitioning decreases (i.e., the densities in the network and in bulk become more similar) with increasing adsorbate density. Clearly the partitioning increases for denser matrices, i.e., with increasing $\rho_N \sigma^3$. Also shown in Fig. 6 are the MC simulation results of Fanti and Glandt.[16] Reasonable agreement with the current theoretical curves can be observed. Deviations exist for high η^r, where the theoretical
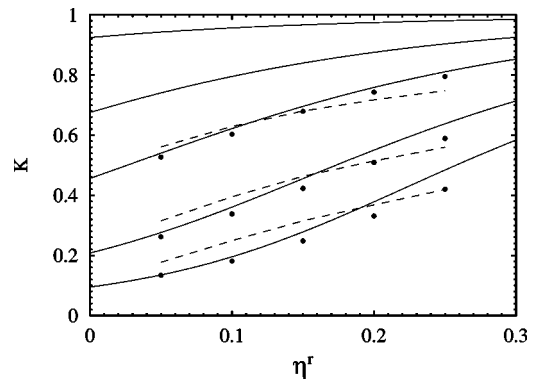
FIG. 6. Partition coefficient $K = \eta/\eta^r$ of spheres of packing fraction η in the random fiber network in chemical equilibrium with a pure hard sphere reservoir of packing fraction η^r for size ratio $L/\sigma = \infty$ and scaled needle densities $\rho_N \sigma^2 L = 0.1, 0.5, 1, 23$ (from top to bottom). Results from the current theory (solid lines) are compared to MC simulation data of Ref. 17 (symbols) and the single-fiber superposition approximation of Ref. 16 (dashed lines).

curves overestimate the MC results for K. This effect, that the DFT gives slightly too weak partitioning, was also apparent in the plateau values of the inhomogeneous density profiles above. The agreement of our results with the MC data of Ref. 17 and that of the results from single-fiber superposition approximation of Ref. 16 is comparable, although the current approach fares somewhat better in predicting the curvature correctly, especially at high matrix densities.

We return to the case of fibers with finite length and display results in Fig. 7 for K as a function of η^r for size ratio $L/\sigma = 2$ and over a broad range of densities, $\rho_N \sigma^3 = 0.1, 0.2, 0.5, 1, 2, 5, 10$. For high needle densities remarkable crossover behavior is observed. Consider $\rho_N \sigma^3 = 5$, where for small packing fractions ($\eta < 0.1$) practically no spheres will enter, but for $\eta > 0.2$ a pronounced increase with η^r occurs. Using such a porous medium as an efficient filter for the hard sphere fluid would require one to keep the reservoir fraction below this crossover region.

It turns out that a natural measure for the needle density is $\rho_N \mathcal{E}_{SN}$. For the needle densities above corresponding nu-
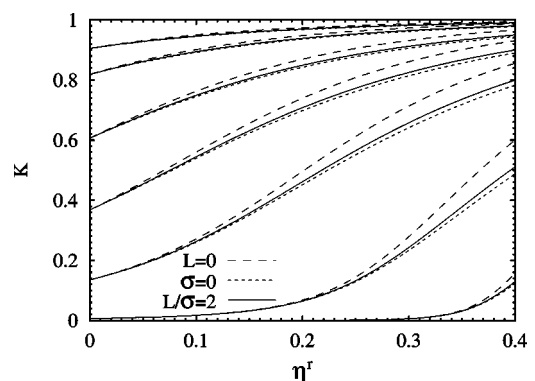
FIG. 7. Same as Fig. 6 but for size ratio $L/\sigma = 2$ and needle densities $\rho_N \sigma^3 = 0.1, 0.2, 0.5, 1, 2, 5, 10$ (solid lines, from top to bottom). For comparison also the corresponding results for $L/\sigma = 0$ and $L/\sigma = \infty$ are shown; densities are such that the needle density times the sphere-needle pair excluded volume, $\rho_N \mathcal{E}_{SN}$, is the same as for the curves for $L/\sigma = 2$.

merical values are $\rho_N \mathcal{E}_{SN} = 0.209\,44$, $0.418\,879$, 1.0472, 2.0944, $4.188\,79$, 10.472, 20.944. We now change the size ratio L/σ while keeping $\rho_N \mathcal{E}_{SN}$ constant. An almost complete data collapse is obtained, see Fig. 7 for results for the extreme cases $L/\sigma = 0, \infty$. The size ratio $L/\sigma = 0$ corresponds to a matrix of randomly distributed hard point particles. Interestingly, the corresponding adsorption, η, is only slightly larger than that for $L/\sigma = 2$ over the entire η^r range considered. The curves for infinitely long needles, $L/\sigma = \infty$, lie slightly below the corresponding results for $L/\sigma = 2$, but this is also only a small effect. We conclude that the adsorption behavior of the hard sphere fluid inside a random fiber network is ruled by the needle density, ρ_N, scaled with the sphere-needle pair excluded volume, $\mathcal{E}_{SN}$.

VI. CONCLUSIONS

In conclusion, we have developed and tested a DFT for the hard sphere fluid adsorbed in a quenched matrix of vanishingly thin needles. We find that theoretical density profiles near the surface of a needle matrix agree well with results from our computer simulations. This demonstrates that within the geometrically based DFT different extensions (orientational degrees of freedom[29,30] and treating quenched-annealed mixtures[34]) can be systematically combined.

We have dealt with the most simplistic model in the context using randomly placed needles and disregarding their explicit connectivity. In a real fiber network, contacts between neighboring fibers lead to mechanical stability, whereas in the present model, the needles are somewhat artificially frozen in space. Nevertheless, we expect this simple model to capture the main effects. Note that the excluded volume that is not accessible to a test sphere will have a connected pore structure due to overlapping sphere-needle excluded volumes from different needles. Furthermore we have also ignored correlations between rods that stem from finite rod diameter and hence finite rod–rod excluded volume. This is a common assumption. One could however, treat rod–rod interactions on the Onsager (second virial) level using the techniques developed in Ref. 30, i.e., angular convolutions to build weighted densities.

Our theory can treat nonisotropic fiber distributions. By assuming a needle one-body distribution that explicitly depends on orientation one could model, e.g., brush-like structures. Also mixtures of needles with different lengths should be readily accessible. Further very interesting questions concern phase transitions like the demixing phase behavior of a binary fluid confined in random fiber networks. We expect this to be accessible within the current DFT framework (see Ref. 35). Another interesting question concerns the size selectivity that should occur when immersing two (or more) differently sized hard sphere fluids in the random fiber net-

work. This opens further possibilities to study fiber networks acting as mesoscopic filters.

[1] L. D. Gelb, K. E. Gubbins, R. Radhakrishnan, and M. Sliwinska-Bartkowiak, Rep. Prog. Phys. **62**, 1573 (1999).
[2] G. A. Vliegenthart and H. N. W. Lekkerkerker, J. Chem. Phys. **111**, 4153 (1999).
[3] G. H. Koenderink, G. A. Vliegenthart, S. G. J. M. Kluijtmans, A. van Blaaderen, A. P. Philipse, and H. N. W. Lekkerkerker, Langmuir **15**, 4693 (1999).
[4] A. P. Philipse and A. M. Wierenga, Langmuir **14**, 49 (1998).
[5] A. Wierenga, A. P. Philipse, H. N. W. Lekkerkerker, and D. V. Bogner, Langmuir **14**, 55 (1998).
[6] P. M. Johnson and C. M. van Kats (private communication).
[7] S. G. J. M. Kluijtmans, G. H. Koenderink, and A. P. Philipse, Phys. Rev. E **61**, 626 (2000).
[8] A. P. Philipse and S. G. J. M. Kluijtmans, Physica A **274**, 516 (1999).
[9] E. A. J. F. Peters, M. Kollmann, T. A. O. M. Barenbrug, and A. P. Philipse, Phys. Rev. E **63**, 021404 (2001).
[10] A. P. Philipse, Langmuir **12**, 1127 (1996), **12**, 5971 (1996).
[11] S. Williams and A. P. Philipse, Phys. Rev. E **67**, 051301 (2003).
[12] C. T. J. Dodson and W. W. Sampson, Appl. Math. Lett. **10**, 87 (1997).
[13] C. T. J. Dodson and W. W. Sampson, J. Stat. Phys. **96**, 447 (1999).
[14] K. Lin, J. C. Crocker, A. C. Zeri, and A. G. Yodh, Phys. Rev. Lett. **87**, 088301 (2001).
[15] P. Bolhuis and D. Frenkel, J. Chem. Phys. **101**, 9869 (1994).
[16] L. A. Fanti and E. D. Glandt, J. Colloid Interface Sci. **135**, 385 (1990).
[17] L. A. Fanti and E. D. Glandt, J. Colloid Interface Sci. **135**, 397 (1990).
[18] L. J. Frink, A. G. Salinger, M. P. Sears, J. D. Weinhold, and A. L. Frischknecht, J. Phys.: Condens. Matter **14**, 12167 (2002).
[19] J. Shen and P. A. Monson, Mol. Phys. **100**, 2031 (2002).
[20] A. G. Ogston, Trans. Faraday Soc. **54**, 1754 (1958).
[21] A. G. Ogston, Biophys. Chem. **57**, 3 (1995).
[22] R. Evans, Adv. Phys. **28**, 143 (1979).
[23] R. Evans, in *Fundamentals of Inhomogeneous Fluids*, edited by D. Henderson (Dekker, New York, 1992), p. 85.
[24] Y. Rosenfeld, Phys. Rev. Lett. **63**, 980 (1989).
[25] R. Roth, R. Evans, A. Lang, and G. Kahl, J. Phys.: Condens. Matter **14**, 12063 (2002).
[26] J. A. Cuesta, Y. Martinez-Raton, and P. Tarazona, J. Phys.: Condens. Matter **14**, 11965 (2002).
[27] Y. Rosenfeld, Phys. Rev. E **50**, R3318 (1994).
[28] Y. Rosenfeld, Mol. Phys. **86**, 637 (1995).
[29] M. Schmidt, Phys. Rev. E **63**, 050201(R) (2001).
[30] J. M. Brader, A. Esztermann, and M. Schmidt, Phys. Rev. E **66**, 031401 (2002).
[31] P. G. Bolhuis (private communication).
[32] R. Evans, J. Phys.: Condens. Matter **2**, 8989 (1990).
[33] W. Dong, E. Kierlik, and M. L. Rosinberg, Phys. Rev. E **50**, 4750 (1994).
[34] M. Schmidt, Phys. Rev. E **66**, 041108 (2002).
[35] M. Schmidt, E. Schöll-Paschinger, J. Köfinger, and G. Kahl, J. Phys.: Condens. Matter **14**, 12099 (2002).